

Neutron emission for the fusion of $^{40}\text{Ar} + \text{Ni}$, ^{92}Mo , ^{122}Sn reactions at $E/A = 26$ MeV

K. Yoshida,* J. Kasagi, H. Hama,† M. Sakurai,‡ M. Kodama,§ and K. Furutaka
Department of Physics, Tokyo Institute of Technology, 2-12-1 Oh-okayama, Meguro, Tokyo 152, Japan

K. Ieki**
Department of Physics, Rikkyo University, Toshima, Tokyo 171, Japan

W. Galster††
University of Tsukuba, Ibaraki 305, Japan

T. Kubo and M. Ishihara‡‡
RIKEN (The Institute of Physical and Chemical Research), Wako-shi, Saitama 351-01, Japan

A. Galonsky
Physics Department and Cyclotron Laboratory, Michigan State University, East Lansing, Michigan 48824
 (Received 20 March 1992)

In order to study the properties of hot nuclei, neutrons emitted in the $^{40}\text{Ar} + \text{Ni}$, ^{92}Mo , ^{122}Sn reactions at $E/A = 26$ MeV were measured in coincidence with fusion residues. The neutron spectra obtained for different residue velocities were analyzed with the moving source model. The spectra are well reproduced with two sources; one corresponds to preequilibrium emission and the other to the decay of fusion nuclei. The extracted neutron multiplicity and initial temperature of the fusion nuclei indicate the formation of thermally equilibrated nuclei with excitation energy up to 5.0 MeV/nucleon. The extracted relation between the temperature and the excitation energy shows that the level densities of the hot nuclei are well described with the level density parameter $a = A/(9 \pm 1)$ for excitation energies from 2.5 to 5.0 MeV/nucleon.

PACS number(s): 25.70. -z, 25.70.Jj

I. INTRODUCTION

Intermediate-energy nucleus-nucleus collisions have provided a unique opportunity to produce hot nuclei. Measurements of linear momentum transfer indicate that nuclei with excitation energies of up to ~ 6 MeV/nucleon can be produced by fusion reactions [1,2]. The nuclear level density of such hot nuclei is one of the interesting subjects to study. Holub *et al.* [3] and Hilscher *et al.* [4] have deduced the level density from neutron spectra measured in the $^{20}\text{Ne} + ^{165}\text{Ho}$ reaction at $E/A = 11, 14.6, 20.1,$ and 30 MeV. Their detailed comparison between

experimental spectra and statistical calculations led to the result that the level density of highly excited nuclei with mass number $A \sim 180$ was well described with the level density parameter $a = A/(10.5 \pm 1.0)$ for excitation energies (E_x) from 1 to 3 MeV/nucleon. Chbihi *et al.* [5] recently reported the level density for $A \sim 110$ by comparing proton and deuteron spectra measured in the $^{28}\text{Si} + ^{100}\text{Mo}$ reaction at $E/A = 25$ MeV with statistical model calculations. The result shows that the level density parameter is about $A/10 - A/11$ for excitation energies between 1.3 and 3.0 MeV/nucleon.

On the other hand, a different conclusion on the level density parameter was deduced by Nebbia *et al.* [6] from α -particle spectra measured in the $^{14}\text{N} + ^{154}\text{Sm}$ reaction at $E/A = 19$ and 35 MeV. The relation they obtained between temperature and excitation energy shows that the level density parameter a decreases from $A/8$ to $A/13$ as the excitation energy increases from 0.6 to 2.5 MeV/nucleon. At higher excitation energies, Fabris *et al.* [7] reported that α -emission temperatures were almost constant for E_x between 2 and 4.3 MeV/nucleon. This observation requires the level density parameter to increase from $A/13$ to $A/10$. Similar results were also reported by Wada *et al.* [8] from the measurements of charged particles emitted in the $^{16}\text{O}, ^{32}\text{S} + \text{Ag}$ reactions at $E/A = 30$ MeV/nucleon.

These observations stimulated much theoretical work on the level density of hot nuclei. In a naive picture, the level density parameter becomes $A/16$, which is expected

*Present address: RIKEN (The Institute of Physical and Chemical Research), Wako-shi, Saitama 351-01, Japan.

†Present address: Ultraviolet Synchrotron Orbital Radiation Laboratory, Institute for Molecular Science, Myodaiji, Okazaki 444, Japan.

‡Present address: Kita-Itami Works, Mitsubishi Electric Co. Ltd., Itami, Hyogo, Japan.

§Present address: Sony Co., Shinagawa, Tokyo 141, Japan.

**Present address: National Superconducting Cyclotron Laboratory, Michigan State University, East Lansing, MI 48824.

††Present address: Universite Catholique de Louvain, Chemin du Cyclotron 2, B-1348 Louvain-La-Neuve, Belgium.

‡‡Also at Department of Physics, University of Tokyo, Hongo, Tokyo 113, Japan.

in the pure Fermi gas model, since the residual interaction and the pair correlation become less important at high excitation energies. However, temperature-dependent Hartree-Fock calculations [9,10] show that the level density parameter a stays almost constant up to about $T=5$ MeV, and then slightly increases at higher temperatures. Although a decrease of a with excitation energy is obtained in several calculations [11–15], the predicted variations in a are much smaller than those reported in Refs. [6–8].

In order to understand the properties of hot nuclei, it is important to obtain systematic information on the level density for a wide range of masses and excitation energies. It is of particular interest to measure neutrons emitted from nuclei with excitation energies between 3.0 and 5.0 MeV/nucleon, where a strong variation of the level density parameter was reported in the measurements of α particles. There are some difficulties in studying hot nuclei. Since nucleus-nucleus collisions at intermediate energy initiate many reaction processes, the excitation energies of the reaction products are widely distributed from low to high excitation energies. Thus, the fusion process should be selected to eliminate the effects of other processes which produce nuclei with lower excitation energies. In addition, the observed spectrum contains information not only on the hot nuclei but also on the nuclei with low excitation energies as a result of the decay of hot nuclei. It is necessary to estimate the effect of the decay cascade and to eliminate it from the observed spectrum.

In this paper we report on measurements of neutrons in coincidence with fusion residues in the $^{40}\text{Ar} + \text{Ni}$, ^{92}Mo , and ^{122}Sn reaction at $E/A=26$ MeV. By measuring both complete and incomplete fusion processes with these beam-target combinations, we were able to make a systematic study of hot nuclei with E_x between 2.5 and 6.0 MeV/nucleon for $A \sim 80, 120, \text{ and } 140$. Coincident measurements with heavy residues made it possible to separate the fusion process from the others. The excitation energies of primary products could be deduced from the velocities of the residues together with a subtraction of energy lost in the pre-equilibrium stage. Part of the results for the $^{40}\text{Ar} + ^{92}\text{Mo}$ reaction has been reported in Ref. [16].

II. EXPERIMENT

Neutrons were measured in coincidence with fusion residues from reactions of $^{40}\text{Ar} + \text{Ni}$, ^{92}Mo , and ^{122}Sn at $E/A=26$ MeV. Self-supported foils of Ni, ^{92}Mo , and ^{122}Sn with thickness of 1.7, 1.9, and 1.0 mg/cm², respectively, were irradiated with ^{40}Ar beams from the RIKEN Ring Cyclotron. The maximum energy loss of the fusion residues in the targets is about 10% for the worst case. The beam size at the target was maintained less than 2 mm in diameter during the run. In order to reduce the background, beams were dumped in a shielded Faraday cup located 10 m downstream from the target. The target chamber is made of stainless steel and its thickness is 1 cm. The attenuation of neutrons in the chamber wall is about 26 and 18% for neutrons with energies 5 and 50

MeV, respectively, and the effect was corrected in the off-line analysis.

As described in Ref. [16], the fusion residues were detected with an annular Parallel-plate avalanche counter (PPAC), which was located at 35 cm from the target and covered angles from 6.5° to 9.7° with respect to the beam axis. The detection efficiency for the evaporation residues was estimated to be about 30% from the systematics of angular distributions of evaporation residues [17]. The PPAC measured both the time of flight (TOF) of the residues and their energy loss. The TOF was measured against rf pulses from the cyclotron. The TOF resolution was mainly limited by the time resolution of the beam and was about 0.7 ns.

The neutrons were observed with seven NE213 scintillation detectors positioned at 32°, 47°, 66°, 83°, 107°, 132°, and 157° with respect to the beam axis. Four backward detectors were 20 cm in diameter and 5 cm in thickness and were located at 100 cm from the target. The remaining three detectors were 12 cm in diameter and 5 cm in thickness and, in order of increasing detection angle, were located at 180, 120, and 110 cm from the target. A brass plate of 5 mm thickness was placed just in front of each neutron detector to prevent charged particles from hitting the detector. In this configuration, protons with energies below 125 MeV stopped before the detectors.

The in-beam background of scattered neutrons was measured with shadow bars placed between the neutron detectors and the target. They are brass cylinders 15 cm in diameter and 30 and 40 cm in length. The longer bar was used for the three forward detectors. The background neutrons were measured for two detectors at the same time. Two shadow bars were placed, firstly, at 32° and 83° so as to cover the full solid angles subtended by the respective detectors, while the other detectors were in use for the measurements without a shadow bar. After that, the shadow bars were moved for the other set of detectors placed at 47° and 107°, and then at 66° and 132°. The background measurement for 157° detector was made separately. More than 99% of the neutrons with $E_n \leq 50$ MeV are attenuated by the bars. The contribution of neutrons scattered by shadow bar for neighboring detector was estimated to be less than 0.5% of those directly coming from the target. Actually, a comparison of spectra without any shadow bars to those with a shadow bar for the neighboring detector does not discern any statistically significant difference. Therefore, the two spectra were combined into one.

The hardware threshold of each detector was set at about 0.5 MeV electron equivalent energy (MeVee). In the off-line analysis the threshold was increased to the value of 1 MeVee in order to decrease the background. The detection efficiency was calibrated for neutron energies of $15 < E_n < 30$ MeV at the TOF facility at Tohoku University. The thick target yields of neutrons from the reaction of $^9\text{Be}(p,n)^9\text{B}$ at $E_p=35$ MeV were measured and compared to those obtained with the calibrated detector. The deduced efficiency for the threshold setting of 9 MeVee was compared to calculations with the code TOTEFF [18], since the efficiency for the threshold at 1 MeVee could not be obtained due to the contribution of

low-energy neutrons arising from the preceding beam burst. The calculated results were consistent with measured ones within $\pm 10\%$ for the threshold at 9 MeVee. Thus, the efficiency for the threshold at 1 MeVee was obtained by multiplying the calculated ratio for the 1 and 9 MeVee setting by the measured efficiency at 9 MeVee.

Figure 1 shows the TOF spectrum for the neutron detector before rejecting the γ -ray events. The spectrum consists of a sharp peak of γ rays and a broad bump of neutrons. The time resolution of the NE213 detector, which is deduced from the width of the γ -ray peak, was 1.2 ns. This time resolution corresponds to an energy resolution of about ± 0.2 and ± 5.5 MeV for the neutron energies of 5 and 50 MeV, respectively. With the γ -ray peak as a time reference, the neutron residue TOF was obtained, and by adding the computed residue TOF, the neutron TOF and then energy was generated. The in-beam background measured with the shadow bar is also shown in Fig. 1 with a thin line. The broad bump of the background events shifts to the lower-energy side, as expected, and the yield of the background is about 10% of the total for most of the energy region. The background was subtracted from the spectrum without the shadow bar. The γ -ray events were eliminated by selecting the neutron events on a two-dimensional spectrum of pulse height versus pulse shape. The contribution of chance coincidences between the NE213 and the PPAC was less than 5%.

High-energy protons with energies above 125 MeV can penetrate into the neutron detector after passing through the wall of the target chamber, air, the brass absorber, and the front face of the container of the liquid scintillator, and, thus, might contaminate the neutron spectra for $E_n > 70$ MeV. In order to check the contribution of these protons, pulse height spectra of the neutron detectors were generated for three TOF bins corresponding to neutron energies of 70–80, 80–90, and 90–100 MeV, and

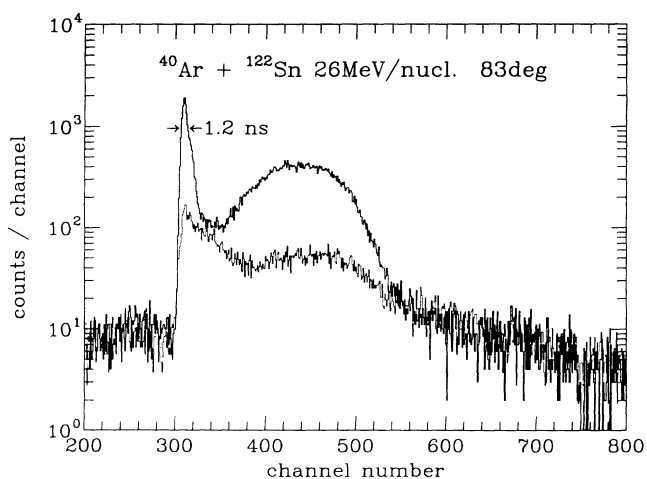


FIG. 1. Time-of-flight spectrum of neutrons and γ rays detected at 83° in the $^{40}\text{Ar} + ^{122}\text{Sn}$ reaction. The thin line indicates the background spectrum measured with the shadow bar. TOF resolution determined from the γ ray peak is also shown in the figure.

yields in the windows of the spectra for the estimated deposit energies of protons (5–35, 35–53, and 53–65 MeV for respective bins) were examined. They were 30 ± 10 , 27 ± 11 , and $20 \pm 15\%$ of total yields, respectively. Although they were consistent with the calculated portions of the neutron pulse height spectra, the events in the windows were not included in final spectra.

III. DATA ANALYSIS AND RESULTS

A. Residue spectra

Figure 2 shows two-dimensional plots (energy loss versus TOF) for the residues in the $^{40}\text{Ar} + \text{Ni}$, ^{92}Mo , and ^{122}Sn reactions. Two groups of events are seen in the figure for each reaction. One corresponds to the peripheral events, which have low-energy losses in the PPAC and velocities near the beam velocity. The other corresponds to the fusion events, which have large-energy losses and velocities below the complete fusion velocity. They are clearly separated for the $^{40}\text{Ar} + ^{92}\text{Mo}$ and ^{122}Sn reactions, as seen in the figure. For the $^{40}\text{Ar} + \text{Ni}$ reaction, however, the separation is rather worse, since the complete fusion velocity is closer to the beam velocity and the residue masses are also closer to the projectile mass in comparison with the other reactions. For all three targets, the residue velocities corresponding to the maximum yield of fusion events are lower than the one expected from the complete fusion (V_{CF}). The velocities at these maxima are 86%, 73%, and 74% of that of V_{CF} for the $^{40}\text{Ar} + \text{Ni}$, ^{92}Mo , and ^{122}Sn reactions, respectively. The value for the $^{40}\text{Ar} + ^{122}\text{Sn}$ reaction is in good agreement with the most probable velocity of fusion residues in the $^{40}\text{Ar} + ^{124}\text{Sn}$ reaction at $E/A = 27$ MeV reported in Ref. [19].

As can be seen in Fig. 2, the velocity distribution of the fusion residues spreads widely from the full to 40% of V_{CF} . The spread due to recoils of evaporated particles is

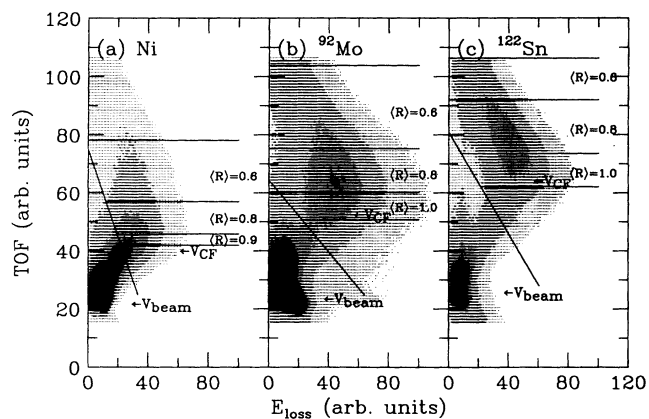


FIG. 2. Two-dimensional spectra (TOF vs energy loss) of the residues measured with the PPAC for the (a) $^{40}\text{Ar} + \text{Ni}$, (b) ^{92}Mo , and (c) ^{122}Sn reactions at $E/A = 26$ MeV. The center of the velocity windows of the residues used in the analysis of the neutron spectra is shown with the ratio ($\langle R \rangle$) of the average of the observed velocity to complete fusion velocity.

estimated to be about 20% in complete fusion reactions [17], and energy loss in the target spreads the velocity only about 5%. Thus, the observed velocity distribution is mainly caused by the distribution of the linear momentum transfer (LMT) of the fusion reactions. In order to select the linear momentum transfer, velocity windows of 105–85%, 85–65%, and 65–45% of the V_{CF} were set on the observed residue velocities. Each bin was represented by the ratio R between the average velocity of the window $\langle V_{obs} \rangle$ and the complete fusion velocities ($\langle R \rangle = \langle V_{obs} \rangle / V_{CF}$). The window width was taken comparable to the width of residue velocity distribution from particle evaporation. Because of the poor separation between the peripheral and the fusion events for the $^{40}\text{Ar} + \text{Ni}$ reaction, a window with $\langle R \rangle = 0.9$ (95–85% of V_{CF}) was used instead of $\langle R \rangle = 1.0$ in order to avoid possible contamination from the peripheral events. The window boundaries are shown as the solid lines in Fig. 2 with the $\langle R \rangle$ value.

B. Neutron spectra

The coincidence between evaporated particles and residues may impose a kinematical bias on the particle spectra. This is due to the fact that the observed velocity of residues and the velocity of evaporated particles are related to each other through the recoil effect. Before analyzing the experimental data, we performed a statistical model simulation to evaluate the effect. By using the Monte Carlo version of the code CASCADE [20], the coincidence spectrum with the actual experimental geometry was generated and compared with the inclusive one and it was found to be biased. One of the causes arises from the limited angular acceptance of the residue detector. Residues emitted close to 0° , which is the most probable direction, are not detected with the present geometry of the PPAC. We only detected residues in the tail region of the angular distribution. This affects the coincident particle spectrum in principle. However, quantitative comparison shows that the effect is negligible for the present geometry, because the PPAC provides a rather large solid angle and axial symmetry with respect to the beam axis. However, the selection of a specific residue velocity causes a non-negligible effect on the evaporated particle spectrum. Because of the recoil effect, the residues have larger (smaller) velocity than the average one when the emitted particle is detected at backward (forward) angles in the center of mass system. Thus, setting a gate on the same observed residue velocity for different angles of the emitted particles is not a correct method to specify the initial momentum of the residues. This kinematical bias should be eliminated by taking into account the recoil of the observed particles. The velocity \mathbf{V}_i of the residue after emitting the i th particle is obtained as

$$M_i \mathbf{V}_i = M_{i-1} \mathbf{V}_{i-1} - m_i \mathbf{v}_i = M_{i-1} \mathbf{V}_{i-1} - m_i (\bar{\mathbf{v}}_i + \mathbf{V}_{i-1}), \quad (1)$$

where M_i is the mass of the residue after the i th particle emission and m_i ($= M_{i-1} - M_i$) and \mathbf{v}_i are the mass and

the velocity of the i th emitted particle, respectively. $\bar{\mathbf{v}}_i$ denotes the velocity of the particle in the emitter frame. The relation between \mathbf{V}_i and \mathbf{V}_{i-1} is

$$\mathbf{V}_i = \mathbf{V}_{i-1} - \frac{m_i}{M_i} \bar{\mathbf{v}}_i. \quad (1')$$

The final velocity of the residue is then obtained by using Eq. (1') recurrently,

$$\mathbf{V}_R = \mathbf{V}_0 - \sum_{i \neq j} \frac{m_i}{M_i} \bar{\mathbf{v}}_i - \frac{m_j}{M_j} \bar{\mathbf{v}}_j, \quad (2)$$

where \mathbf{V}_R and \mathbf{V}_0 are the velocities of the final residue and the initial nucleus. The subscript j denotes the observed particle in coincidence with the residue. The summation terms gives the spread of the residue velocity from the recoil of evaporated particles. This term does not depend on the particle observed in coincidence with the residues. We get the initial velocity \mathbf{V}_0 with the ambiguity of the velocity spread,

$$\mathbf{V}_0 - \sum_{i \neq j} \frac{m_i}{M_i} \bar{\mathbf{v}}_i = \mathbf{V}_R + \frac{m_j}{M_j} \bar{\mathbf{v}}_j. \quad (2')$$

Since the statistical emission is isotropic, the left-hand side of Eq. (2') gives $\langle \mathbf{V}_0 \rangle$ when we take an ensemble average. After transforming from the center-of-mass frame to the laboratory frame, we get the relation of

$$\begin{aligned} \langle \mathbf{V}_0 \rangle &= \mathbf{V}_R + \left\langle \frac{m_j}{M_j} \mathbf{v}_j - \frac{m_j}{M_j} \mathbf{V}_{j-1} \right\rangle \\ &\sim \mathbf{V}_R + \frac{m_j}{\langle M_j \rangle} \mathbf{v}_j - \frac{m_j}{\langle M_j \rangle} \langle \mathbf{V}_0 \rangle. \end{aligned} \quad (3)$$

Thus we obtain the relation

$$\langle \mathbf{V}_0 \rangle \sim \frac{\langle M_j \rangle \mathbf{V}_R + m_j \mathbf{v}_j}{\langle M_{j-1} \rangle}. \quad (4)$$

We used $\langle \mathbf{V}_0 \rangle$ as the most probable estimation of \mathbf{V}_0 in the analysis. The value of $\langle M_j \rangle$ is assumed to be the mean residue mass during the decay cascade. The values used are 80, 120, and 135 for the $^{40}\text{Ar} + \text{Ni}$, ^{92}Mo , and ^{122}Sn reactions, respectively. These values are estimated from the average excitation energy and the mass of the fused nuclei. This correction was made in the off-line analysis with the event-by-event mode.

The neutron spectra after the correction for measured efficiency and subtraction of the background are shown in Figs. 3–5 for various windows of the residue velocities. These spectra mainly consist of two exponentially falling components. The slopes of the spectra become steeper with increasing detection angle. In order to compare the spectra in their emitting frame, the neutron spectra were parametrized in terms of the thermal moving source model [21]. In the model, the Maxwellian shape is assumed as the energy distribution of the neutrons. It is also assumed that the neutrons are emitted isotropically in the emitting frame. The energy distribution in this frame of the source is given by

$$\frac{d^2\sigma}{dE_n d\Omega} = \frac{M}{2(\pi\tau)^{3/2}} \sqrt{E_n} \exp\left[-\frac{E_n}{\tau}\right], \quad (5)$$

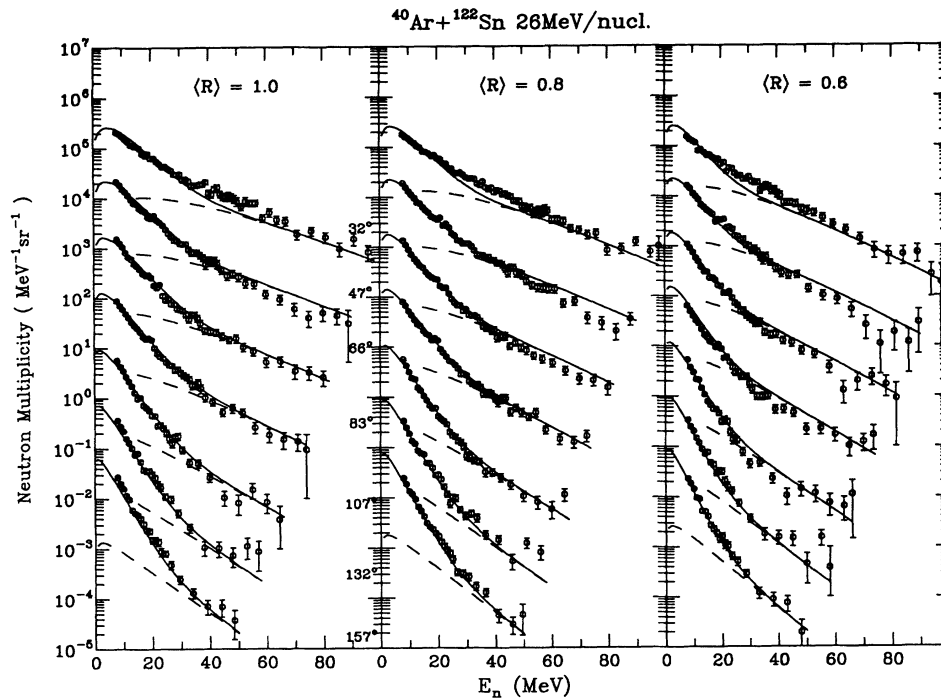


FIG. 3. Neutron spectra in coincidence with residues of various velocities, given by $\langle R \rangle = \langle V_{\text{obs}} \rangle / V_{CF}$, from the $^{40}\text{Ar} + ^{122}\text{Sn}$ reaction. The solid curves are the results of fits with two moving sources, and the dashed curves are contributions of pre-equilibrium emission. The spectra at 32° , 47° , 66° , 83° , 107° , 132° , and 157° are multiplied by 10^n , with n being 6, 5, 4, 3, 2, 1, and 0, respectively.

where M is the multiplicity of neutrons, E_n is the kinetic energy of the neutron, and τ is the source temperature parameter. Two sources are used to describe the experimental spectrum. One source is the fusion source, which corresponds to neutron emission after the composite sys-

tem has achieved the thermal equilibrium. The other is a pre-equilibrium source, which corresponds to neutron emission before the whole system has reached thermal equilibrium. The fitting function of the neutron spectra was then obtained by transformation from the emitting

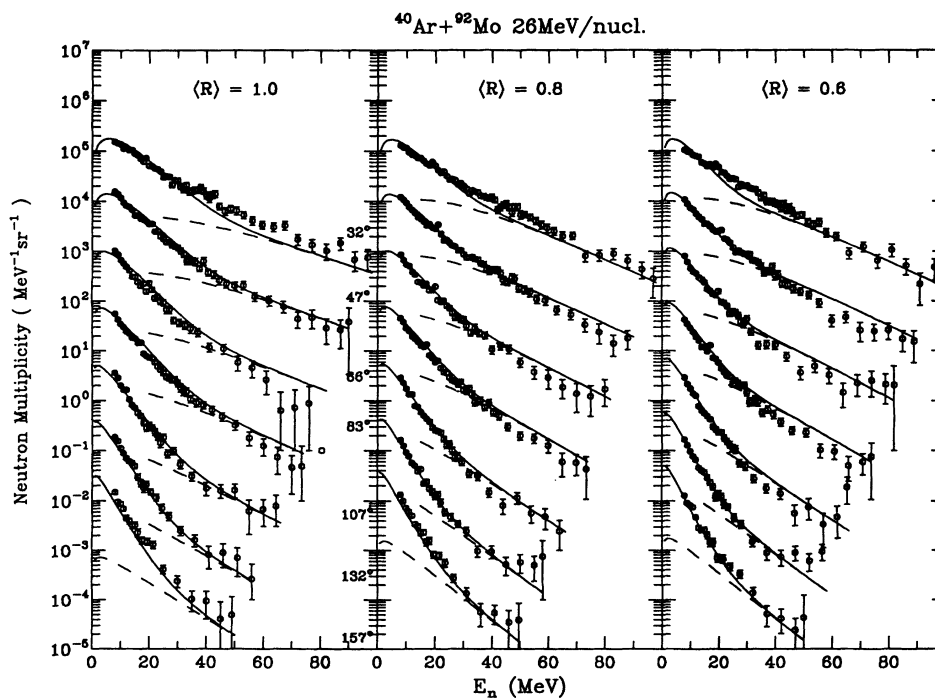
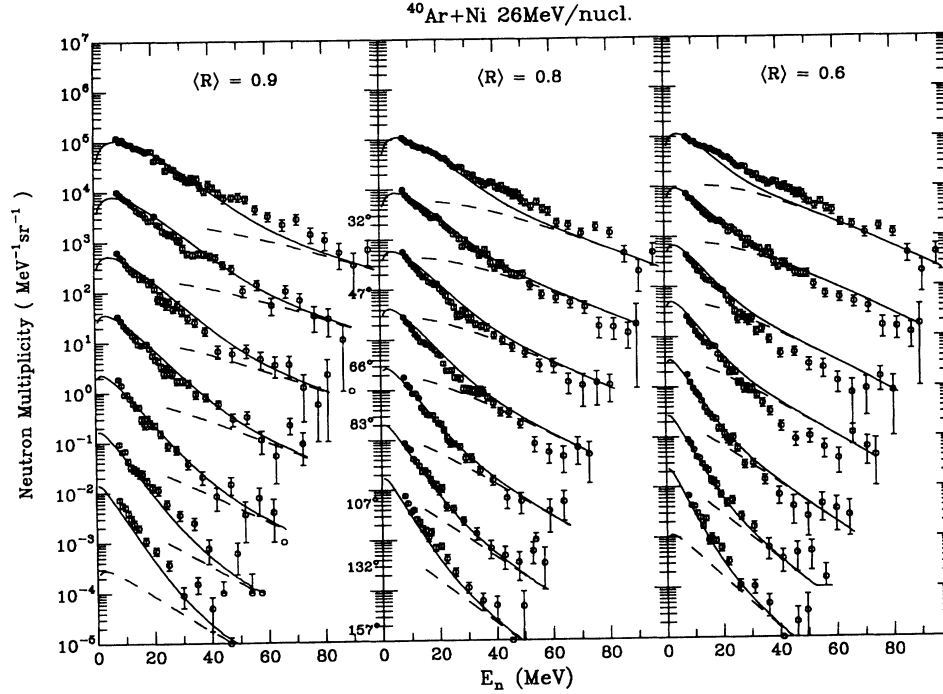


FIG. 4. Same as Fig. 3 for the $^{40}\text{Ar} + ^{92}\text{Mo}$ reaction.

FIG. 5. Same as Fig. 3 for the $^{40}\text{Ar} + \text{Ni}$ reaction.

frame to the laboratory frame:

$$\frac{d^2\sigma}{dE_n d\Omega} = \sum M_i \frac{\sqrt{E_n}}{2(\pi\tau_i)^{3/2}} \exp\left[-\frac{E_s}{\tau_i}\right], \quad (6)$$

where

$$E_s = E_n - 2\sqrt{\varepsilon_i E_n} \cos(\theta) + \varepsilon_i, \quad (7)$$

E_n is the neutron kinetic energy, and θ is the neutron detection angle in the laboratory frame. M_i and τ_i are the associated neutron multiplicity and temperature parameter for each source, respectively, and ε_i is the kinetic energy per nucleon of the source, which is assumed to move on the beam axis. In the fitting procedure, the velocity of the fusion source was fixed at the average resi-

due velocity of each bin. The data with energies below 5 MeV were not employed, since the detection efficiency for the low-energy neutrons depends strongly on the threshold energy and hence includes large ambiguity.

The multiplicity, the temperature parameter, and the velocity of the pre-equilibrium source deduced from the fitting are summarized in Table I. The multiplicity and the temperature parameter of the fusion source increase as the $\langle R \rangle$ value ($= \langle V_{\text{obs}} \rangle / V_{CF}$) increases. This fact indicates that the excitation energy of fusion products increases with increasing linear momentum transfer. The results of the fitting with two sources are shown by the solid lines in Figs. 3–5, and the contribution of the pre-equilibrium source is shown by the dashed lines. It can be said that the observed spectra are well reproduced by

TABLE I. Parameters obtained in the fitting with the two-source moving source model for the different residue velocity bins.

$\langle R \rangle$	M_{eq}	τ_{eq} (MeV)	M_{pre}	τ_{pre} (MeV)	V_{pre}/V_p
			$^{40}\text{Ar} + ^{122}\text{Sn}$		
1.0	20.5 ± 2.7	4.78 ± 0.31	2.1 ± 0.6	13.6 ± 1.7	0.58 ± 0.07
0.8	19.1 ± 2.7	4.33 ± 0.28	2.5 ± 0.5	12.4 ± 1.1	0.54 ± 0.05
0.6	17.1 ± 2.8	3.82 ± 0.31	2.6 ± 0.6	11.1 ± 0.8	0.45 ± 0.08
			$^{40}\text{Ar} + ^{92}\text{Mo}$		
1.0	13.7 ± 1.9	5.22 ± 0.37	1.1 ± 0.5	15.0 ± 3.1	0.58 ± 0.09
0.8	11.4 ± 1.8	4.52 ± 0.36	1.9 ± 0.6	11.8 ± 1.2	0.51 ± 0.05
0.6	11.1 ± 1.8	4.05 ± 0.33	1.9 ± 0.4	11.7 ± 0.9	0.49 ± 0.04
			$^{40}\text{Ar} + \text{Ni}$		
0.9	9.3 ± 1.0	6.12 ± 0.57	0.5 ± 0.7	15.8 ± 3.9	0.65 ± 0.10
0.8	8.3 ± 1.1	5.29 ± 0.41	1.1 ± 0.5	13.1 ± 2.1	0.58 ± 0.08
0.6	7.1 ± 1.1	4.31 ± 0.35	1.6 ± 0.4	11.1 ± 0.09	0.57 ± 0.05

the model of two moving sources. The spectra at 32° , however, are systematically underestimated in the fitting. This might suggest the existence of another source which has a strongly forward-peaked angular distribution in the laboratory system. A possibility is the projectilelike source, which represents the neutrons emitted from an unobserved part of a projectile which passes through the target.

C. Pre-equilibrium source parameter

The derived multiplicity and temperature parameters of the pre-equilibrium source contain large errors, since, in the present experiment, the neutrons were measured at rather backward angles. Nevertheless, the following trends can be pointed out in the present work. The multiplicity of pre-equilibrium emission M_{pre} increases with decreasing residue velocity. This dependence of M_{pre} on $\langle R \rangle$ becomes weaker as the target mass increases. These features can also be shown for other systems when we compare the results of the $^{20}\text{Ne} + ^{165}\text{Ho}$, $^{32}\text{S} + \text{Ag}$, and $^{16}\text{O} + \text{Ag}$ reactions at $E/A = 30$ MeV [4,8]. For the heaviest system, M_{pre} is almost independent of residue velocity, whereas it is weakly increasing with decreasing residue velocity for the other two systems.

The temperature parameter τ_{pre} seems to be independent of the target mass but weakly dependent on the $\langle R \rangle$ values. A similar $\langle R \rangle$ dependence is seen in the neutron spectra for the $^{20}\text{Ne} + ^{165}\text{Ho}$ reaction [4] and in the charged particle spectra for the ^{32}S , $^{16}\text{O} + \text{Ag}$ reactions [8] at $E/A = 30$ MeV. The values of τ_{pre} are also in good agreement with the systematics for the beam energy obtained from neutron-residue coincidence measurements [22].

The velocity of the pre-equilibrium source V_{pre} is almost independent of target mass and is about 50–60% of the beam velocity. Although similar results were reported for the $^{20}\text{Ne} + ^{165}\text{Ho}$ and ^{32}S , $^{16}\text{O} + \text{Ag}$ reactions [4,8], the $\langle R \rangle$ dependence of V_{pre} is different. In the present work V_{pre} slightly increases with increasing R , while, the V_{pre} reported in Ref. [8] is almost constant and the V_{pre} reported in Ref. [4] decreases with increasing residue velocity.

D. Excitation energies and temperatures of the fusion products

The excitation energy of the equilibrated fusion nuclei has been estimated using the assumption that the whole target merges with a part of the projectile and the remaining part of the projectile passes through with its initial velocity. In this assumption, momentum and energy conservation give the mass A_{eq} , the velocity V_R , and the excitation energy E_{eq}^* of the fusion nuclei as

$$A_{\text{eq}} = A_p + A_t - \sum_i M_{\text{pre}}^i A^i - \Delta A, \quad (8)$$

$$V_R = \frac{A_p V_p - \sum_i M_{\text{pre}}^i A^i V_{\text{pre}} - \Delta A V_p}{A_{\text{eq}}}, \quad (9)$$

and

$$E_{\text{eq}}^* = \frac{1}{2} A_t V_p V_R - \frac{1}{2} \sum_i M_{\text{pre}}^i A^i (V_p - V_{\text{pre}})(V_R - V_{\text{pre}}) - \frac{3}{2} \sum_i M_{\text{pre}}^i \tau_{\text{pre}} + Q, \quad (10)$$

where A_p , A_t , ΔA , V_p , V_{pre} , τ_{pre} , and Q are the mass number of the projectile, target, and the unobserved part of the projectile, the velocity of the beam, and the pre-equilibrium source, the temperature parameter of the pre-equilibrium source, and the reaction Q value, respectively. The Q value is estimated by using the assumption that the unobserved part of the projectile travels as a cluster in its ground state. M_{pre}^i and A^i are the multiplicity and the mass of the particles emitted from the pre-equilibrium source. Emission of neutrons, protons, deuterons, tritons, and α particles is considered from the pre-equilibrium source. The multiplicity of the protons M_{pre}^p is estimated from M_{pre}^n and the N/Z ratio of the fused nucleus. The multiplicities of d , t , and α particles are estimated as $\frac{1}{2}M_{\text{pre}}^p$, $\frac{1}{4}M_{\text{pre}}^p$, and $\frac{1}{2}M_{\text{pre}}^p$ according to the results of Wada *et al.* [8]. If V_R or ΔA is given, the coupled equation of Eqs. (8)–(10) can be solved using the parameters extracted from the moving source fit. We assumed $\Delta A = 0$ for $\langle R \rangle = 1.0$ window and for the other cases, we used the observed velocity (V_{obs}) as V_R . The thermal excitation energies of nuclei after one neutron emission are then deduced using the following relation:

$$E_{\text{th}} = E_{\text{eq}}^* - S_n - \langle \epsilon r \rangle - \frac{\hbar^2 J^2}{2I}, \quad (11)$$

where S_n is the separation energy of the neutron and $\langle \epsilon \rangle$ is the average kinetic energy removed by the neutron. The fourth term is the rotation energy of the daughter nucleus with moment of inertia I and angular momentum J . The angular momentum was estimated with an abrasion-absorption model [23]. The estimated J values were $(20-35)\hbar$, $(40-55)\hbar$, and $(55-70)\hbar$ for the $^{40}\text{Ar} + \text{Ni}$, ^{92}Mo , and ^{122}Sn reactions, respectively, and hence the rotation energies are 10–35 MeV for these reactions. The excitation energies of the daughter nuclei are summarized in Table II together with the average linear momentum transfer (LMT) and the average masses of the equilibrated nuclei.

The initial temperature T of the daughter nuclei can be deduced from the temperature parameter τ . The relation between τ and T has been obtained by Le Couteur and Lang [24] as $T = (12/11)\tau$ when the fitting function $E^{5/11} \exp(-E/\tau)$ is used for the neutron energy distribution. However, this approximation is only valid for neutrons emitted from the states at lower excitation energies. Instead of using this relation, we derived the relation numerically for neutron emission from highly excited nuclei by using the code CASCADE with an assumption that the level density parameter a is independent of the excitation energy. The calculation was performed with $a = A/8$ and $A/12$ for the $^{40}\text{Ar} + ^{92}\text{Mo}$ reaction for various excitation energies. The calculated spectra were fitted with the function $\sqrt{E} \exp(-E/\tau)$ and the deduced τ was com-

TABLE II. Derived values of excitation energies and temperatures of the fused nuclei.

$\langle R \rangle$	LMT	ΔA	A_{eq}	E_{eq}^* (MeV)	E_{th} (MeV)	T (MeV)
				$^{40}\text{Ar} + ^{122}\text{Sn}$		
1.0	94%	0	153	556	520	5.50 ± 0.35
0.8	71%	5	146	451	399	4.98 ± 0.32
0.6	47%	12	138	357	305	4.39 ± 0.36
				$^{40}\text{Ar} + ^{92}\text{Mo}$		
1.0	97%	0	127	575	544	6.00 ± 0.43
0.8	61%	9	114	405	356	5.20 ± 0.41
0.6	43%	14	109	326	275	4.66 ± 0.38
				$^{40}\text{Ar} + \text{Ni}$		
0.9	87%	3	92	521	496	7.04 ± 0.66
0.8	61%	10	83	389	350	6.08 ± 0.47
0.6	36%	17	72	259	211	4.96 ± 0.40

pared with the T obtained from the relation $E_{\text{th}} = aT^2$. The relation obtained is shown in Fig. 6. The solid line represents the relation $T = (12/11)\tau$, which is actually a good approximation, but only for $\tau < 3.0$ MeV. For $\tau > 3.0$ MeV, the slope gets larger with increasing τ , and the relation $T = 1.15\tau$, which is shown by the dashed line, becomes a good approximation for $\tau > 4.0$ MeV. This behavior can be understood by the fact that more charged particles are emitted at high excitation energies than at low excitation energies. The factor 1.15 is in agreement with results recently reported by Chbihi *et al.* [5]. The initial temperatures obtained are listed in Table II.

In Fig. 7 we plot the initial temperature T against exci-

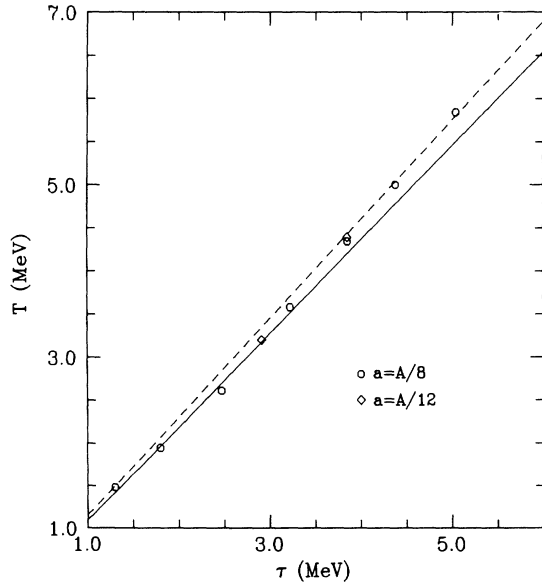


FIG. 6. The relation of the initial temperature T to the temperature parameter τ deduced from statistical calculations with the level density parameter $a = A/8$ (circles) and $a = A/12$ (diamonds). τ is obtained by fitting the calculated spectrum with $\sqrt{E} \exp(-E/\tau)$, whereas the initial temperature T is defined by the relation $E_{\text{th}} = aT^2$. Solid and dashed lines show the relation $T = \frac{12}{11}\tau$ and $T = 1.15\tau$, respectively.

tation energy per nucleon for the $^{40}\text{Ar} + \text{Ni}$ (squares), ^{92}Mo (circles), and ^{122}Sn (diamonds) reactions. The temperature increases smoothly with increasing excitation energy. As seen in the figure, the temperature-excitation energy relation is well described with the level density parameter of $a = A/(9 \pm 1)$ for all the targets. The neutron multiplicities of the fusion source are plotted against the excitation energy in Fig. 8. The multiplicity obtained from the statistical calculation with a constant level density parameter $a = A/9$ is also shown as solid lines in the figure. Neutron, proton, and α -particle emissions are considered in the calculation performed with the code CASCADE. The optical potentials of Wilmore and Hodgson [25], Perey [26], and Mcfadden and Satchler

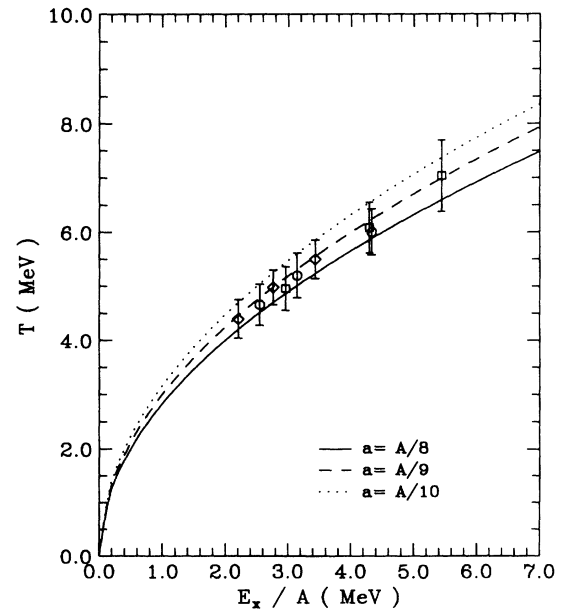


FIG. 7. Initial temperature vs excitation energy per nucleon obtained in the $^{40}\text{Ar} + \text{Ni}$ (squares), ^{92}Mo (circles), and ^{122}Sn (diamonds) reactions. The solid, dashed, and dotted curves correspond to the level density parameter $a = A/8$, $A/9$, and $A/10$, respectively.

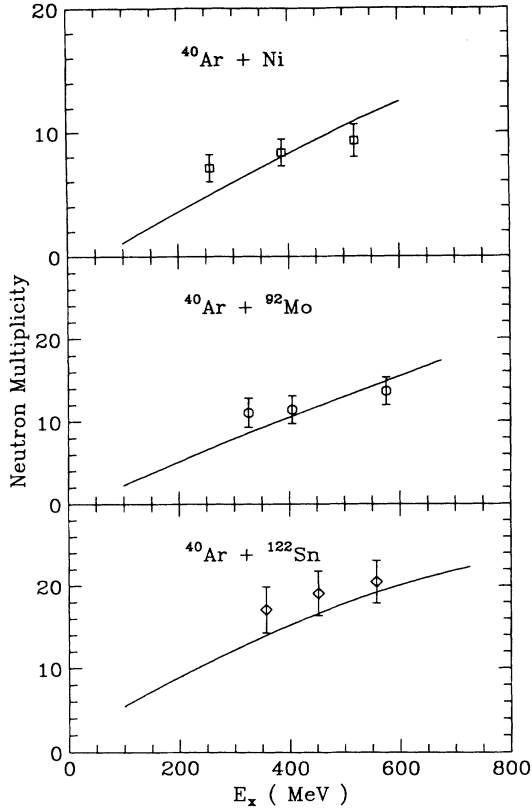


FIG. 8. Neutron multiplicity of the fusion nuclei produced in the $^{40}\text{Ar} + \text{Ni}$, ^{92}Mo , and ^{122}Sn reactions as a function of excitation energy. Solid lines represent the statistical model calculations with level density parameter $a = A/9$.

[27] were used for calculating the transmission coefficients for neutrons, protons, and α particles, respectively. It can be seen that the multiplicity is reasonably reproduced by the calculation. These facts indicate that the equilibrated nuclei are formed through the fusion reaction at the excitation energies up to 3.4, 4.3, and 5.4 MeV/nucleon for masses around 150, 130, and 90, respectively. However, the agreement in Fig. 8 is not complete. For all three targets, the increase of multiplicity with E_x is slower for the data than for the calculation.

IV. DISCUSSION

The level density parameters obtained in the present analysis do not depend strongly on the excitation energy, but can be described as $a = A/(9 \pm 1)$ up to an excitation energy of 5 MeV/nucleon. This agrees with the results of Refs. [3] and [4] in which the level density parameter is found to have a constant value of $A/(10.5 \pm 1.0)$ between 1 and 2 MeV/nucleon. Thus, based on the neutron measurements, it can be said that the level density of hot nuclei can be described with the Fermi gas distribution with $a \sim A/10$ and the excitation energy dependence of a is not large enough to be observed. On the other hand, a different conclusion has been deduced in Refs. [6–8] based on the α -particle measurements. The authors in Refs. [6–8] claimed that the level density parameter de-

creases from $A/8$ to $A/13$ for excitation energies from 1 to 2 MeV/nucleon and increases from $A/13$ to $A/10$ for 3 to 4 MeV/nucleon. They obtained the initial temperature essentially by subtracting the effects of lower excitation energies and, hence, the contribution of the emission from the nuclei in deexcitation cascade seems to be removed.

It should be mentioned here that the deduction of the level density parameter a from the relation $E_x = aT^2$ is not always correct. Thermodynamically the temperature T is defined as

$$1/T = d(\ln \rho) / dE_x, \quad (12)$$

where ρ is the level density. If a does not depend on E_x , the Fermi gas description of ρ gives the relation of $E_x \approx aT^2$. On the other hand, if a does depend on E_x , the quantity da/dE_x appears in the relation between T and E_x , and the simple law $E_x = aT^2$ is no longer a valid. In order to deduce the value of a in this case, firstly, the level density ρ should be obtained using the relation

$$\rho = \exp \left[\int \frac{1}{T} dE_x \right]. \quad (13)$$

Figure 9 shows the relation between the level density and the excitation energy. Using the relation between T and E_x reported in Refs. [6–8] together with the assumption of $a = A/8$ for $E_x < 180$ MeV, we have evaluated the level density by Eq. (13) and plotted it with the solid line in Fig. 9. The dotted lines are the level density of Fermi gas obtained simply from the relation $E_x = aT^2$ for

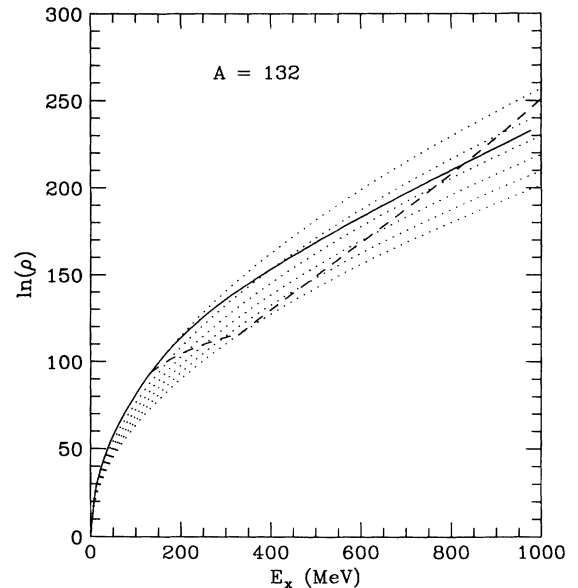


FIG. 9. Relation between the level density (ρ) and excitation energy (E_x). Dotted curves show the simple Fermi gas approximation with a fixed level density parameter $a = A/k$ for $k = 8, 9, 10, 11, 12$, and 13 . The solid line shows the realistic relation evaluated with the data of Refs. [6–8], whereas the dashed line represents an interpretation with $E_x = aT^2$ given in Refs. [6–8].

$a = A/8 - A/13$. The deduced level density deviates from the value for $a = A/8$ above $E_x \sim 200$ MeV, but increases, monotonically to the value for $a = A/10$ at $E_x \sim 1000$ MeV. For comparison, the dashed line shows the interpretation that a changes from $A/8$ to $A/13$ for E_x from 0.6 to 2.5 MeV/nucleon and increases from $A/13$ to $A/10$ for E_x from 3 to 6 MeV/nucleon. Obviously, this interpretation cannot reproduce the experimentally obtained temperature; it gives a much higher temperature for E_x between 180 and 380 MeV and a much lower temperature for E_x above 400 MeV, since the temperature is defined as $1/T = d(\ln\rho)/dE_x$. Therefore, the real excitation energy dependence of a is much smaller than reported in Refs. [6–8].

In order to see the effect of the variation of the level density parameter on the neutron spectrum, statistical calculations were performed with the level density varied according to the solid line in Fig. 9. In Fig. 10, the experimental spectra for $\langle R \rangle = 1.0$ and 0.6 obtained in the $^{40}\text{Ar} + ^{92}\text{Mo}$ reaction are shown in the center-of-mass frame after subtraction of the pre-equilibrium emissions. The solid lines are the calculations with a constant level density parameter $a = A/8$ and the dashed line is the one with the level density varied as the dashed line in Fig. 9. The fact that the calculation with $a = A/8$ reproduces the data very well proves the present analysis to be correct, since the temperature-excitation energy relation obtained requires a to be close to $A/8$ for $\langle R \rangle = 1.0$ and 0.6 for the ^{92}Mo target as already shown in Fig. 7. The calculated spectra with the varied level density show less

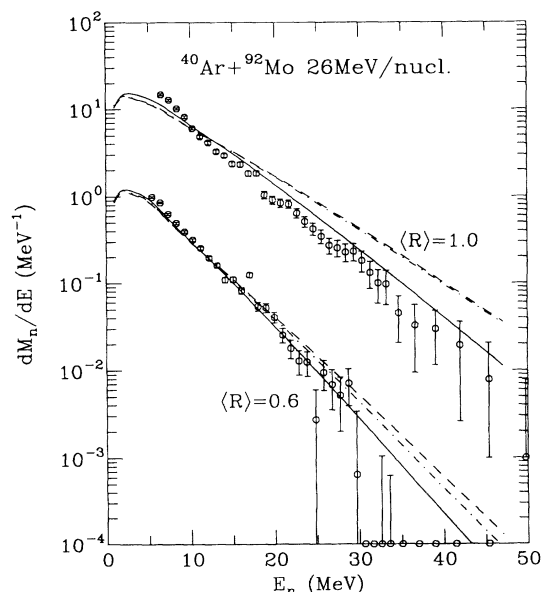


FIG. 10. Evaporated neutron spectra in the emitting frame obtained in the $^{40}\text{Ar} + ^{92}\text{Mo}$ reaction after subtraction of pre-equilibrium emission. The standard statistical calculations with fixed level density parameter are shown for $a = A/8$ with solid lines. The calculation with the level density evaluated with the result of Refs. [6–8] (plotted in Fig. 9 with the dashed line) and result from Ref. [13] are shown with the dashed and dot-dashed lines, respectively.

steep slopes than that of $a = A/8$. For $\langle R \rangle = 0.6$, the difference between the two calculations is not large and the experimental spectrum can be explained for both calculations. As shown in Fig. 9, the variation of the level density incorporated in the calculation corresponds to a small variation of a from $A/8$ to $A/9$. Thus it can be said that the present data cannot show the effect of such a small variation of a . However, the calculated spectrum for $\langle R \rangle = 1.0$ is less steep than the experimental one. This indicates that the variation of a is smaller than the variation of from $A/8$ to $A/9.5$.

The recent study of Chbihi *et al.* [5] shows that the difference in the angular momentum distributions at different excitation energies causes another problem. The study shows that an additional correction is required to remove the angular momentum effect. The correction factors are about 0.9 for neutrons and protons and 0.8 for α particles for the $^{10}\text{B} + ^{100}\text{Mo}$ reaction. If this correction is applied to the temperature parameter obtained in Refs. [6–8], the reported deviation of the level density parameter again becomes smaller than reported.

There have been extensive theoretical discussions on the variation of the level density parameter. Bonche *et al.* [9] studied the level density of hot nuclei with the temperature-dependent Hartree-Fock (HF) method. Instead of the phenomenological single-particle spectra, they used the solution of the HF equation at finite temperatures and deduce the level density with the help of the thermodynamical relation. Although their result does not reproduce the absolute value of a , the variation of a is essentially constant for $T = 2-8$ MeV. Similar results are reported by Suraud *et al.* [10]. A decrease of a with excitation energy has been discussed in the relation of the level density parameter to the effective mass. Hasse and Schuck [13] calculated the temperature dependence of a up to $T = 12$ MeV. Their result with a local Woods-Saxon potential shows that a varies from $A/7$ to $A/10$ for temperatures of 2–7 MeV. Dean and Mosel [11] showed that a must decrease with increasing excitation energy because of the finiteness of single-particle space of nucleus. They predicted that a varies from $A/13$ to $A/17$ for $E_x/A = 2-5$ MeV. Their calculation also failed to reproduce absolute values of a . In both calculations, a changes its value by about 20% for $E_x/A = 4-7$ MeV.

V. SUMMARY AND CONCLUSION

Coincidence measurements between residues and neutrons were performed for the reactions $^{40}\text{Ar} + \text{Ni}$, ^{92}Mo , and ^{122}Sn at $E/A = 26$ MeV. In order to remove the effect of pre-equilibrium emission, neutron spectra were analyzed with the moving source model for different residue velocities with the correction of the recoil effect. The dependence of the extracted parameters of the pre-equilibrium emission on the mass number and the residue velocity was deduced: The temperature does not depend on mass but increases from 11 to 15 MeV as $\langle R \rangle$ increases from 0.6 to 1.0; the neutron multiplicity increases with decreasing $\langle R \rangle$, although the dependence on $\langle R \rangle$ becomes weaker as the mass increases; the velocity of the

pre-equilibrium source is about 50% of the beam velocity. These characteristics are consistent with those reported previously.

The multiplicity and the temperature parameter of the neutron emission from the fused nuclei were also deduced. The relation between the initial temperature and the apparent temperature for the neutron emission from hot nuclei was deduced numerically through CASCADE calculations. It is found that the relation $T = (12/11)\tau$ is valid only for $\tau < 3$ MeV, and the relation $T = 1.15\tau$ is a good approximation at higher temperatures. The initial excitation energy of the fused system was kinematically evaluated from the amount of linear momentum transferred to the fusion residue taking into account the pre-equilibrium emission. The extracted neutron multiplicity and the initial temperature increase from $\langle R \rangle = 0.6$ to 1.0. Thus, the neutron emission can be regarded as the decay of the thermally equilibrated fused

system. The initial-temperature versus excitation-energy relation is well explained with the level density parameter $a = A/(9 \pm 1)$ for excitation energies of 2.5–5.0 MeV/nucleon. No strong variation of a has been deduced.

The conclusion that the excitation energy dependence of a is weak is consistent with the results reported for other systems [3–5], except those in Refs. [6–8], for which we have pointed out that the real variation of a should be much smaller than reported. Although the absolute value of a is not always reproduced by the calculations, several calculations predict that the value of a decreases as the excitation energy increases. However, the predicted variation of a is so small that the effect cannot be seen in the present data. In order to deduce such small variations, a more accurate determination of the temperature as well as the excitation energy of the fusion nuclei is required.

-
- [1] M. Conjeaud, S. Harar, M. Mostefai, E. C. Pollaco, C. Volant, Y. Cassagnou, R. Dayras, H. Oeschlar, and F. Saint-Laurent, *Phys. Lett.* **159B**, 244 (1985).
- [2] S. Leray, *J. Phys. (Paris) Colloq. Suppl.* **47**, C4 (1986), and references therein.
- [3] E. Holub, D. Hilscher, G. Ingold, U. Jahnke, H. Orf, and H. Rossner, *Phys. Rev. C* **28**, 252 (1983).
- [4] D. Hilscher, H. Rossner, A. Gamp, U. Jahnke, B. Cheynis, B. Chambo, D. Drain, C. Pastor, A. Giorni, C. Morand, A. Dauchy, P. Stassi, and G. Petitt, *Phys. Rev. C* **36**, 208 (1987).
- [5] A. Chbihi, L. G. Sobotka, N. G. Nicolis, D. G. Sarantites, D. W. Stracencer, Z. Majka, D. C. Hensley, J. R. Beene, and M. L. Halbert, *Phys. Rev. C* **43**, 666 (1991).
- [6] G. Nebbia, K. Hagel, D. Fabris, A. Majaka, J. B. Natowitz, R. P. Schmitt, B. Sterling, G. Mouchaty, G. Berkowitz, K. Strozewski, G. Viesti, P. L. Gonthier, B. Wilkins, M. N. Namboodiri, and H. Ho, *Phys. Lett. B* **176**, 20 (1986).
- [7] D. Fabris, K. Hagel, J. B. Natowitz, G. Nebbia, R. Wada, R. Billerey, B. Cheynis, A. Demeyer, D. Drain, D. Guinet, C. Pastor, L. Vagneron, K. Zaid, J. Alarja, A. Giorni, D. Heuer, C. Morand, B. Viano, C. Mazur, C. Ngo, S. Leray, R. Lucas, M. Ribrag, and E. Tomasi, *Phys. Lett. B* **196**, 429 (1987).
- [8] R. Wada, D. Fabris, K. Hagel, G. Nebbia, Y. Lou, M. Gonnin, J. B. Natowitz, R. B. Billerey, B. Cheynis, A. Demeyer, D. Drain, D. Guinet, C. Paster, J. Alarja, A. Giorni, D. Heuer, C. Morand, B. Viano, C. Mazur, C. Ng6, S. Leray, R. Lucas, M. Ribrag, and E. Tomasi, *Phys. Rev. C* **39**, 497 (1989).
- [9] P. Bonche, S. Levit, and D. Vautherin, *Nucl. Phys. A* **427**, 278 (1984).
- [10] E. Surand, P. Schuck, and R. W. Hasse, *Phys. Lett.* **164B**, 212 (1985).
- [11] R. Dean and U. Mosel, *Z. Phys. A* **322**, 647 (1985).
- [12] A. Lejeune, P. Grange, M. Martzoff, and J. Cugnon, *Nucl. Phys. A* **453**, 189 (1986).
- [13] R. Hasse and P. Schuck, *Phys. Lett. B* **179**, 313 (1986).
- [14] P. F. Bortignon and C. H. Dasso, *Phys. Lett. B* **189**, 381 (1987).
- [15] H. Sato, *Phys. Rev. C* **36**, 785 (1987).
- [16] K. Yoshida, J. Kasagi, H. Hama, M. Sakurai, M. Kodama, K. Furutaka, K. Ieki, W. Galster, T. Kubo, and M. Ishihara, *Phys. Lett. B* **245**, 7 (1990).
- [17] W. Galster, H. Morgenstern, W. Bohne, K. Grabish, and A. Kyanawski, *Proceedings of the Tukuba International Symposium* (World Scientific, Singapore, 1984), p. 248.
- [18] R. J. Kurz, University of California Radiation Lab. Internal Report No. UCR1-11339, 1964 (unpublished).
- [19] H. Nifenecker, J. Blacho, J. Crancon, A. Gizon, and A. Leres, *Nucl. Phys. A* **447**, 533c (1985).
- [20] F. Pühlhofer, *Nucl. Phys. A* **280**, 267 (1977).
- [21] T. C. Awes, S. Saini, G. Poggi, C. K. Gelbke, D. Cha, R. Legrain, and G. D. Westfall, *Phys. Rev. C* **25**, 2361 (1982).
- [22] E. Holub, D. Hilscher, G. Ingold, U. Jahnke, H. Orf, H. Rossner, W. P. Zank, W. U. Schröder, H. Gemmeke, K. Keller, L. Lassen, and W. Lücking, *Phys. Rev. C* **33**, 143 (1986).
- [23] H. Delagrangé and J. Peter, *Nucl. Phys. A* **471**, 111c (1987).
- [24] K. J. Le Couteur and D. W. Lang, *Nucl. Phys.* **13**, 32 (1959).
- [25] D. Wilmore and P. E. Hodgson, *Nucl. Phys.* **55**, 673 (1964).
- [26] F. G. Perey, *Phys. Rev.* **131**, 745 (1963).
- [27] L. McFadden and G. R. Satchler, *Nucl. Phys.* **84**, 177 (1966).

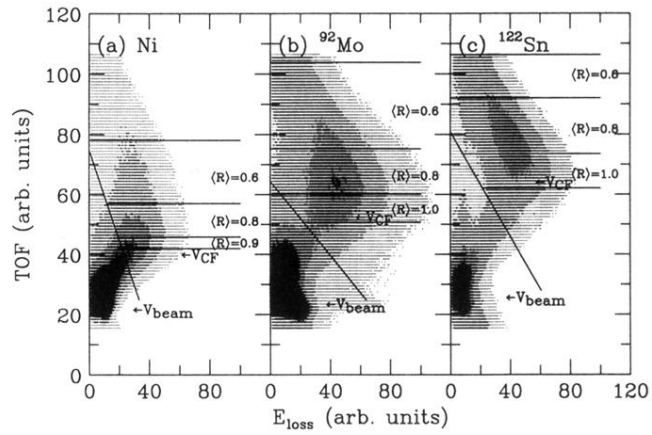


FIG. 2. Two-dimensional spectra (TOF vs energy loss) of the residues measured with the PPAC for the (a) $^{40}\text{Ar}+\text{Ni}$, (b) ^{92}Mo , and (c) ^{122}Sn reactions at $E/A=26$ MeV. The center of the velocity windows of the residues used in the analysis of the neutron spectra is shown with the ratio $\langle R \rangle$ of the average of the observed velocity to complete fusion velocity.